coatings

MDPI

Article

Effect of Trace Elements on the Thermal Stability and Electrical Conductivity of Pure Copper

Haitao Liu *, Jincan Dong, Shijun Liang, Weiqiang Li and Yong Liu

Provincial and Ministerial Co-construction of Collaborative Innovation Center for Non-Ferrous Metal New Materials and Advanced Processing Technology, School of Materials Science and Engineering, Henan University of Science and Technology, Luoyang 471023, China; 18046803380@163.com (J.D.); 13938930573@163.com (S.L.); lwkk0520@163.com (W.L.); liuyong209@haust.edu.cn (Y.L.)

* Correspondence: htliu@haust.edu.cn; Tel.: +86-15538838918

Abstract: The impact of introducing trace transition elements on the thermal stability and conductivity of pure copper was examined through metallographic microscopy (OM), transmission electron microscopy (TEM), and electrical conductivity measurements; the interaction between trace transition element and trace impurity element S in the matrix was analyzed. The results show that the addition of trace Ti and trace Cr, Ni, and Ag elements significantly enhances the thermal stability of the pure copper grain size. After high-temperature treatment at 900 °C/30 min, the grain sizes of Cu, Cu-Ti-S, and Cu-Cr-Ni-Ag-S were measured and found to be 200.24 μm, 83.83 μm, and 31.08 μm, respectively, thus establishing a thermal stability ranking of Cu-Cr-Ni-Ag-S > Cu-Ti-S > Cu. Furthermore, the conductivities of pure copper remain high even after the addition of trace transition elements, with recorded values for Cu, Cu-Ti-S, and Cu-Cr-Ni-Ag-S of 100.7% IACS, 100.2% IACS, and 98.5% IACS, respectively. The enhancement of thermal stability is primarily attributed to the pinning effect of the TiS and CrS phases, as well as the solid solution dragging of Ni and Ag elements. Trace Ti and Cr elements can react with S impurities to form a hexagonal-structure TiS phase and monoclinic-structure CrS phase, which are non-coherent with the matrix. Notably, the CrS phase is smaller than the TiS phase. In addition, the precipitation of these compounds also reduces the scattering of free electrons by solute atoms, thereby minimizing their impact on the alloy's conductivity.

Keywords: pure copper; trace element; thermal stability; conductivity; precipitated phase

Citation: Liu, H.; Dong, J.; Liang, S.; Li, W.; Liu, Y. Effect of Trace Elements on the Thermal Stability and Electrical Conductivity of Pure Copper. *Coatings* **2024**, *14*, 1017. https://doi.org/10.3390/coatings14081017

Academic Editor: Emilio Bellingeri

Received: 3 July 2024
Revised: 7 August 2024
Accepted: 9 August 2024
Published: 10 August 2024

1. Introduction

With the advancement of science and technology, the demand for conductor materials is on the rise [1]. Pure copper, as a crucial conductor material, is extensively utilized in the fields of electronic information, aerospace, new energy vehicles, electrochemistry, and other domains [2–5]. As the mentioned fields progress towards high integration, high power, and miniaturization, the thermal and electrical loads on pure copper materials significantly rise during processing and service. This can lead to abnormally coarse grain sizes in copper materials, affecting their service stability; therefore, higher requirements are put forward for the comprehensive performance of pure copper conductor materials: maintaining high thermal stability while retaining high conductivity [6]. Thermal stability refers to the capacity of a material to endure temperature changes without failure due to grain growth or performance degradation [7]. It is usually hoped that the thermal stability of pure copper grain sizes can withstand high temperatures above 850 °C without significant growth; however, the high purity of pure copper is conducive to the improvement in conductivity, but an increase in purity will also weaken the drag effect of impure atoms on grain boundaries, resulting in unstable grain boundaries. Under heating conditions, the grain boundary diffusion coefficient increases sharply, accelerating grain boundary migration and leading to abnormal grain growth as well as decreased thermal stability [8–10]. Therefore, ensuring the conductivity

and enhancing the thermal stability of copper have gradually become focuses and challenges in recent years. Breaking through the contradiction is crucial for meeting the demand for high-performance pure copper materials in advanced fields [11–16].

Microalloying is an important method for enhancing the thermal stability of copper materials [15,16]. Numerous studies have demonstrated [17–21] that the addition of alloying elements to form high-melting-point particles as crystallization cores or incorporating nano-sized oxides and other strengthening phase particles uniformly into the copper matrix can effectively impede grain boundary migration at elevated temperatures [22,23], thereby improving the thermal stability of pure copper. Commonly added microalloying elements include Cr, Ti, Ag, Sn, and others [24–29]; however, while their addition can enhance the thermal stability of pure copper, they often require high content levels. Additionally, some elements may become solely dissolved in the copper matrix, leading to lattice damage, increased electron wave scattering, and reduced conductivity. This makes it challenging to achieve the synergistic enhancement of both conductivity and thermal stability. For example, when 0.05 mass% Sn is added to pure copper, the high-temperature softening resistance of pure copper significantly improves. The solid dissolution of Sn solute atoms in copper causes lattice distortion, inhibiting grain boundary migration by resisting dislocation slippage, climbing, and reorganization during the high-temperature process; however, when the Sn content is increased to 0.015 mass%, conductivity can be reduced by over 3% IACS [30,31]. Suzuki and Hori [32–35] found that adding trace Ti, Cr, Ag, and Ni elements individually impacts the heat resistance, recrystallization temperature, and electrical conductivity of pure copper. They observed that the effect of improving the thermal stability of pure copper was Ti > Cr > Ag > Ni, but the effect of reducing the electrical conductivity was Ag < Ni < Cr < Ti. Specifically, Ti can increase the softening temperature of pure copper by 200~300 °C, which is about twice as high as that achieved with Cr. The thermal stability increases with the element content, but excessive addition leads to a significant decrease in conductivity. Moreover, pure copper usually contains a certain amount of unavoidable impurity elements, especially sulfur (copper ore mainly exists in the form of sulfide, and electrolytic refining production uses a sulfuric acid-copper sulfate system), which significantly affects the conductivity and thermal stability of pure copper [36–40]. Even a small amount of sulfur, at 15 ppm, in pure copper can lead to a reduction in electrical conductivity to 99.5% IACS. Therefore, it is crucial to achieve synergistic improvement in the conductance and thermal stability of pure copper while minimizing the adverse effects of impurity element sulfur on conductance.

In addition, transition group elements, such as titanium and chromium, exhibit a strong tendency to form sulfides. The Gibbs free energy of sulfide formation by titanium, chromium, and sulfur impurity elements in copper is significantly lower than that of Cu_2S. This suggests the potential for the formation of fine sulfides through the addition of trace amounts of titanium and chromium [29–38]. Furthermore, both titanium and chromium sulfides have high melting points above 1200 °C and demonstrate good thermal stability. They can effectively pin grain boundaries and inhibit grain growth at elevated temperatures. Additionally, reducing the solid solution impurity sulfur content in a matrix can contribute to improved conductivity. At the same time, the addition of alloying elements is very small and there is little solid solution in the matrix, which are conducive to maintaining high conductivity. In addition, the conductivity of pure copper is reduced less by nickel and silver elements, and its thermal stability can be improved by solute dragging in the copper matrix.

In summary, in this paper, the synergistic regulation of the conduction and thermal stability of pure copper is achieved by adding trace Ti alone and combining it with trace Cr, Ni, and Ag elements. This involves using trace transition elements to react with an impurity element, sulfur, to form a micro-nano phase and leveraging the solute dragging effect of trace solid solution elements to alter the occurrence state of an impurity element, sulfur, in copper.

2. Experimental Methods

Pure copper materials with different trace transition elements required by a vacuum induction furnace were smelted under a vacuum and high-purity argon. In the smelting process, 4N electrolytic copper was selected as the raw material, with each furnace weighing 2.5 kg, and the melting temperature was controlled at about 1200 °C. After the copper solution was melted, trace S and trace transition elements, Ti, Cr, Ni, and Ag, were added in the form of a simple substance (the trace elements were wrapped in copper foil and pressed into a block according to the required content in advance to improve the yield, and the purity was 99.99%). After the melting is uniform, a cylindrical ingot with a diameter of Φ80.0 mm was cast. In order to obtain samples with uniform microstructures and properties, the ingot was treated with a high-temperature solution and hot extrusion. The ingot was heated to 950 °C and held for 2 h before being hot-extruded into a copper sheet with a size of 300 mm long × 70 mm wide × 15 mm thick using an XJ-500 extruder. It then air-cooled to room temperature. The thickness of the copper sheet was reduced from its initial 15 mm to 0.5 mm on a two-high rolling mill. Inductively coupled plasma atomic emission spectrometry was used to detect the contents of microalloyed elements. The chemical composition of experimental pure copper with different microalloying elements is shown in Table 1.

Table 1. Chemical composition of experimental pure copper with different microalloying elements (mass fraction, %).

No.	Ti	Cr	Ni	Ag	S	Cu
Cu	<0.0001	<0.0001	0.0001	0.0011	0.0010	Bal.
Cu-Ti-S	0.0035	-	-	-	0.0039	Bal.
Cu-Cr-Ni-Ag-S	-	0.0036	0.0088	0.0030	0.0036	Bal.

The experimental process is shown in Figure 1.

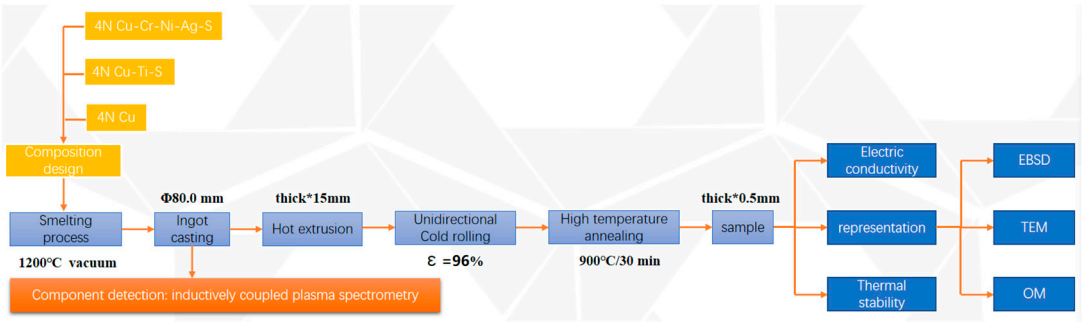

Figure 1. Experimental process.

The sample was intercepted at the same position along the width of the copper plate and tested for electrical conductivity as well as thermal stability. A Sigma 2008B eddy current conductivity meter was used to conduct an electrical conductivity test. The surface of the sample was polished with W5 metallograph sandpaper first, and then the Sigma 2008B eddy current conductivity meter was calibrated and the conductivity of each sample was measured at room temperature, and each sample was tested no less than ten times. After the maximum and minimum values of each sample were removed, the average value obtained is the measured conductivity of the sample. To assess the thermal stability of experimental pure copper, the grain size change before and after high-temperature treatment (900 °C/30 min) was utilized as a criterion. Initially, the sample underwent treatment at 900 °C in a vacuum tube furnace, followed by immediate water cooling after a 30 min hold. Subsequently, both pre and post high-temperature treatment samples were mechanically ground and polished before being subjected to corrosion using a corrosive liquid (composition: 3 g of FeNO3, 15 mL of HCl, 15 mL of distilled water)

for approximately 8 s. Finally, tissue images were captured using an OLYMPUS PMG 3 inverted optical microscope, employing the area method. Image-Pro Plus 6.0 was used to count the total area and number of grains in five photographs taken from different locations on each sample. Subsequently, the average area of a single grain was obtained, allowing for the calculation of the average equivalent diameter of grains as well as a comparison between grain growth before and after high-temperature treatment.

FEI Talos F200X transmission electron microscopy (TEM) and an energy-dispersive spectrometer (EDS) were used to observe the presence of trace transition elements in the cold-rolled copper matrix. After mechanical grinding and electrolysis, TEM samples were further thinned using a Gatan 695 precision ion grinding system under a 3 kV Ar+ ion beam. The precipitated phase was observed and analyzed by TEM, selected area electron diffraction (SAD), and EDS at an acceleration voltage of 200 kV.

3. Results and Analyses

3.1. Effect of Trace Element Interactions on the Electrical Conductivity of Pure Copper

The impact of trace transition group elements on the conductivity of pure copper is illustrated in Figure 2. As can be seen from Figure 2, the addition of trace Ti has minimal influence on the conductivity of pure copper, and the conductivity of Cu-Ti-S pure copper remains above 100% IACS, comparable to that of Cu pure copper. The combined addition of trace Cr, Ni, and Ag can marginally decrease the conductivity of pure copper. The conductivity of Cu-Cr-Ni-Ag pure copper approaches 100% IACS with still-favorable conductivity; however, it is noted that the conductivity of Cu-Cr-Ni-Ag pure copper is lower than that of Cu-Ti pure copper due to high solid solubility effects from Ni and Ag in the copper matrix. Atoms dissolved in the copper matrix will disrupt lattice integrity, increase electron wave scattering, and reduce conductivity. Additionally, because Ni and Ag elements are added in small amounts, their impact on reducing electrical conductivity is limited. In summary, adding microalloying elements such as Ti or Cr, along with Ni and Ag, to pure copper can still ensure high levels of electrical conductivity.

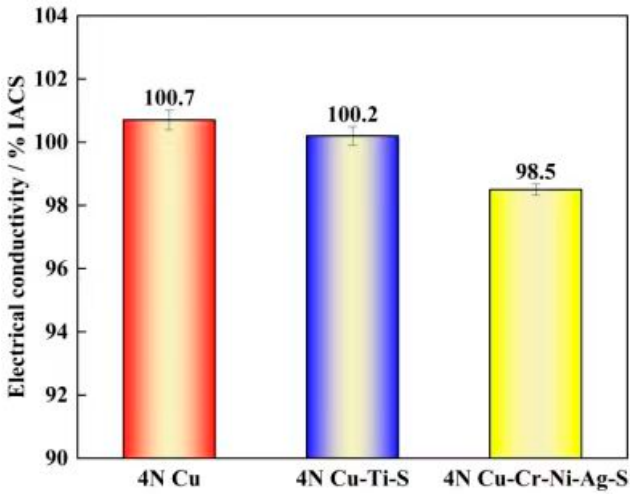

Figure 2. Effect of trace elements on the cold-rolled conductivity of 4N pure copper.

The influence of trace transition group elements on the conductivity of pure copper under various temperatures is depicted in Figure 3. It can be observed from Figure 3 that the conductivity rises with the ascending of temperature ranging from 100 °C to 300 °C. Within the range of 300 °C to 800 °C, the conductivity undergoes a minor fluctuation, yet the fluctuation is relatively insignificant. According to the temperature-dependent study of electrical conductivity (mobility), it is found [41,42] that impurity atoms and lattice vibration will have scattering effects on carriers, hindering their transport and affecting the mobility of carriers, thus affecting the conductivity. At low temperatures, the impurity

scattering and lattice vibration effects are relatively weak, the carrier mobility is higher, and the influence on the conductivity is small, so the conductivity increases linearly with the increase in temperature at low temperatures. With the increase in temperature, the impurity scattering and lattice vibration effects are enhanced, and the carrier mobility is reduced, which has a relatively large impact on the electrical conductivity. Therefore, as the temperature rises, the upward trend of conductivity is not remarkable, and even shows a minor downward tendency.

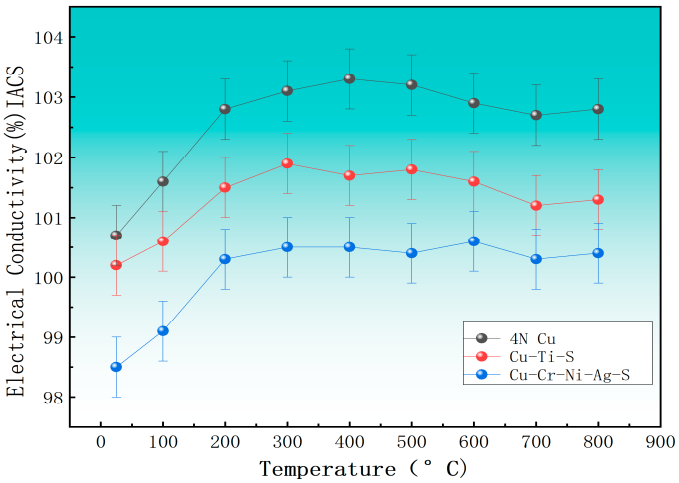

Figure 3. Effect of trace transition group elements on the conductivity of pure copper at different temperatures.

3.2. Effect of Trace Elements on Thermal Stability

Using the conventional cold-rolling process, 4N pure copper with trace transition elements in an extruded state was rolled into a 0.5 mm copper sheet by a two-high rolling mill through multiple passes. Figure 4 shows an optical micrograph of pure copper with a trace amount of transition group element 4N added in a cold-rolled state. As can be seen from Figure 4, after cold-rolling for 4NCu, 4N Cu-Ti-S, and 4N Cu-Cr-Ni-Ag-S pure copper samples for multiple passes, the grain elongation along the rolling direction presents a banded structure.

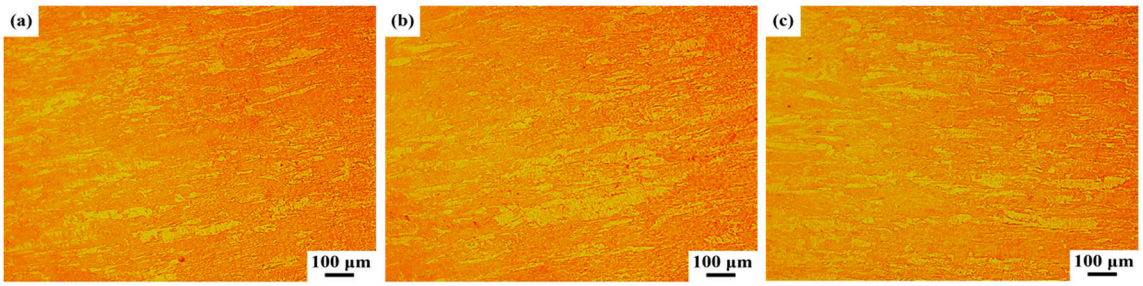

Figure 4. Optical micrographs of pure copper with trace element 4N added in a cold-rolled state: (**a**) optical micrograph of 4Ncu; (**b**) 4N Cu-Ti-S optical micrograph; and (**c**) 4N Cu-Cr-Ni-Ag-S optical micrograph.

Based on the change in grain size after high-temperature treatment at 900 °C/30 min, the influence of trace transition group elements on the thermal stability of pure copper was investigated. Figure 5 shows the optical micrograph and average grain size of cold-rolled 4N pure copper after high-temperature treatment with different trace transition elements. Figure 5 indicates that the addition of trace transition group elements can significantly refine the grain size of pure copper compared to that of pure copper without these additions. After treatment at 900 °C/30 min, it is observed that the grain size of 4N Cu-Ti-S and 4N Cu-Cr-Ni-Ag-S is much smaller than that of 4N Cu, especially with an average grain size as

low as 31.08 μm for 4N Cu-Cr-Ni-Ag-S. Furthermore, post high-temperature heat treatment, it is evident from Figure 5 that the grains in cold-rolled 4Ncu pure copper are coarse, with an average grain size measuring approximately 200.24 μm and individual grains reaching up to 400 μm. Both 4N Cu-Ti-S and 4N Cu-Cr-Ni-Ag-S exhibit significantly smaller grain sizes following high-temperature heat treatment than those of 4N Cu pure copper. The average grain size of 4N Cu-Ti-S is 83.83 μm, which represents a reduction of 58% compared to that of 4N Cu pure copper. Meanwhile, the average grain size of 4N Cu-Cr-Ni-Ag-S measures approximately 31.08 μm, indicating an impressive decrease of 84% in comparison to that of 4N Cu pure copper. These findings demonstrate that the addition of the trace transition group element Ti and the combined addition of trace transition group elements Cr, Ni, and Ag can effectively improve the thermal stability of grain size in cold-rolled 4N pure copper. After high-temperature treatment, the average grain size of 4N Cu-Cr-Ni-Ag-S is only 16% of that of 4N Cu pure copper. This indicates that the compound addition of trace transition elements Cr, Ni, and Ag has the most significant effect on enhancing the thermal stability of cold-rolled pure copper grain size.

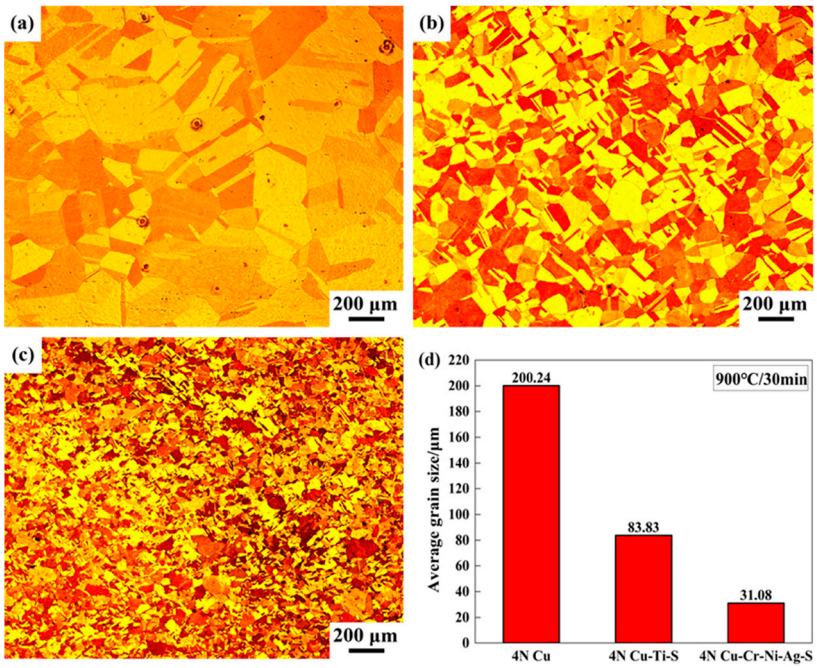

Figure 5. Optical micrograph and average grain size of 4N pure copper with different trace elements added after high-temperature treatment in a cold-rolled state: (**a**) 4Ncu optical micrograph; (**b**) 4N Cu-Ti-S optical micrographs; (**c**) 4N Cu-Cr-Ni-Ag-S optical micrograph; and (**d**) average grain size.

3.3. Changes in Recrystallization Temperature

Figure 6 shows the recrystallization temperature curve of pure copper with different trace transition elements added. As depicted in Figure 6, the addition of trace transition group element Ti and the compound addition of trace transition group elements Cr, Ni, and Ag can effectively elevate the recrystallization temperature of pure copper. The initial hardness of 4N Cu-Ti-S and 4N Cu-Cr-Ni-Ag-S is higher than that of 4N pure copper. The hardness of 4Ncu, 4N Cu-Ti-S, and 4N Cu-Cr-Ni-Ag-S pure copper decreases linearly and slowly at 30~130 °C. Within the range of 130~160 °C, recrystallization occurs in 4N pure copper, leading to a rapid decrease in hardness, while the hardness of 4N Cu-Ti-S and 4N Cu-Cr-Ni-Ag-S decreases slowly. In the range of 160~190 °C, the hardness of 4N Cu-Ti-S and 4N Cu-Cr-Ni-Ag-S pure copper begins to decrease rapidly after recrystallization. Subsequently, the hardness of all three samples tends to stabilize with a slower rate of decline as the annealing temperature is increased. Figure 5 illustrates that the recrystallization

temperature for 4N pure copper falls within the range of 130~160 °C, while for both 4N Cu-Ti-S and 4N Cu-Cr-Ni-Ag-S, it lies in the range of 160~190 °C.

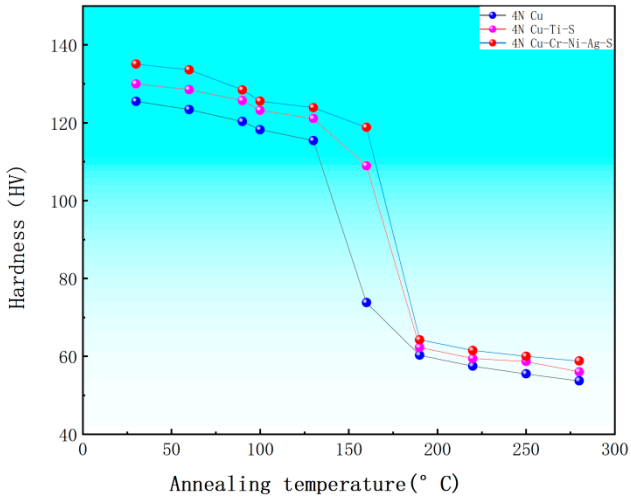

Figure 6. Recrystallization temperature curves of 4N pure copper with different trace elements added.

Figures 7–9 show optical micrographs of 4N pure copper with different trace transition elements added at various annealing temperatures. It can be seen from Figures 7–9 that after annealing at 160 °C/1 h, 4N Cu pure copper has undergone recrystallization, while 4N Cu-Ti-S and 4N Cu-Cr-Ni-Ag-S remain banded. Following annealing at 190 °C/1 h, 4N Cu-Ti-S and 4N Cu-Cr-Ni-Ag-S were recrystallized. Based on the recrystallization temperature curve, it is evident that adding trace transition group element Ti and the compound addition of trace transition group elements Cr, Ni, and Ag can effectively increase the recrystallization temperature of pure copper and further improve its thermal stability.

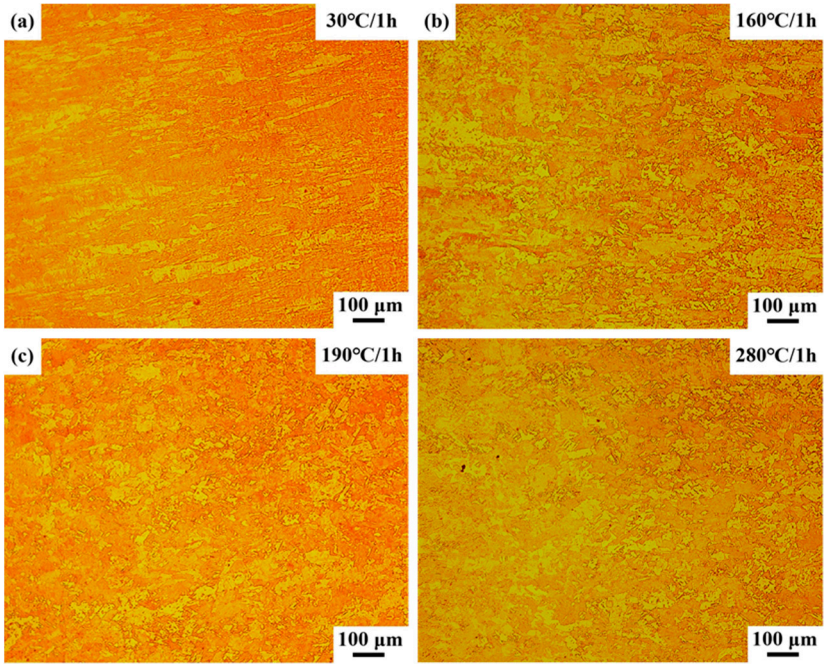

Figure 7. Optical micrographs of 4N Cu pure copper at different annealing temperatures: (**a**) optical micrograph at 30 °C/1 h; (**b**) optical micrograph at 160 °C/1 h; (**c**) optical micrograph at 190 °C/1 h; and (**d**) optical micrograph at 280 °C/1 h.

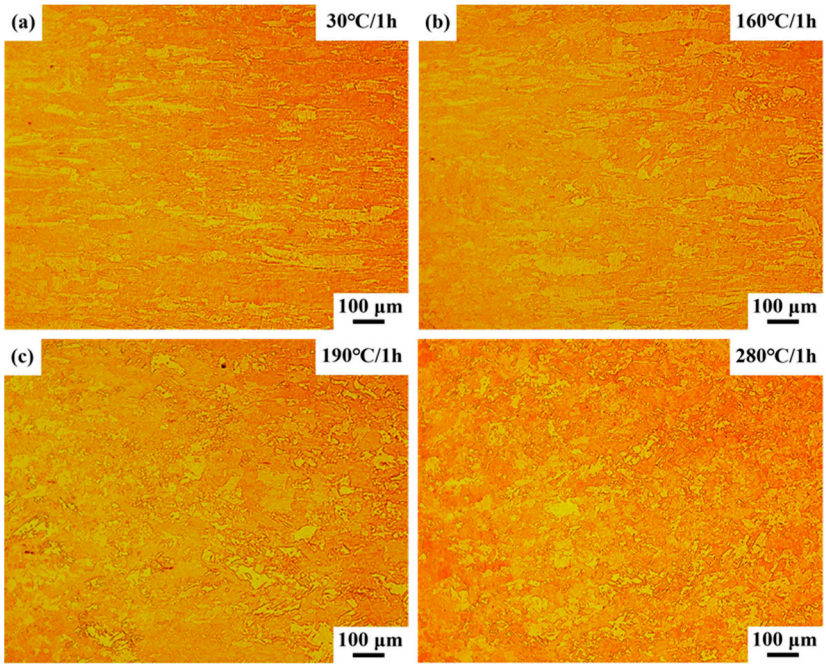

Figure 8. Optical micrographs of 4Ncu-Ti-S at different annealing temperatures: (**a**) optical micrograph at 30 °C/1 h; (**b**) optical micrograph at 160 °C/1 h; (**c**) optical micrograph at 190 °C/1 h; and (**d**) optical micrograph at 280 °C/1 h.

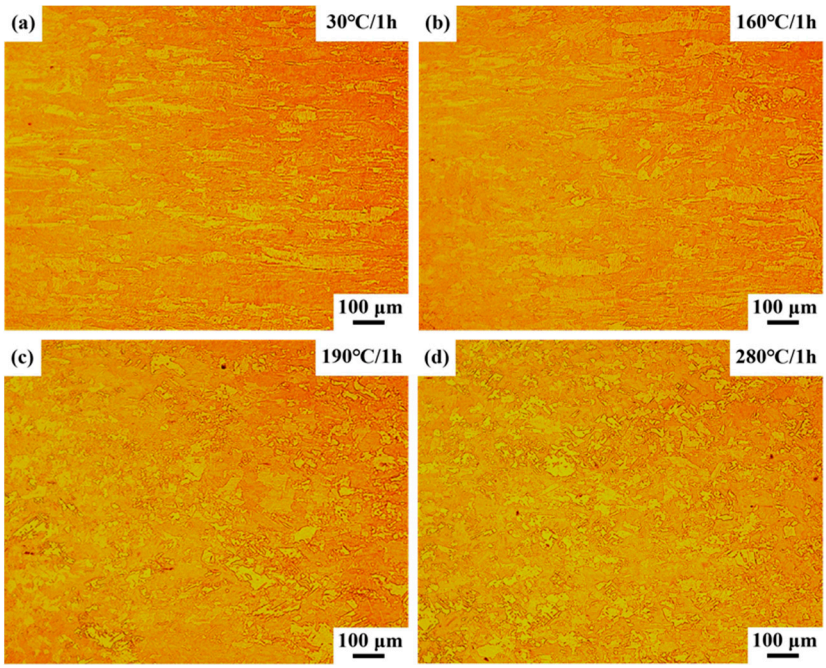

Figure 9. Optical micrographs of 4Ncu-Cr-Ni-Ag-S at different annealing temperatures: (**a**) optical micrograph at 30 °C/1 h; (**b**) optical micrograph at 160 °C/1 h; (**c**) optical micrograph at 190 °C/1 h; and (**d**) optical micrograph at 280 °C/1 h.

3.4. Analysis of the Existence Form of Trace Elements

To clarify the influence of trace elements on the electrical conductivity and thermal stability of pure copper, the forms of added Ti, Cr, Ni, and Ag in cold-rolled pure copper were analyzed using TEM. The results are shown in Figures 10–15. Upon the addition of trace Ti and Cr elements, a reaction with the S element in pure copper occurs, resulting in the formation of the TiS phase and CrS phase in 4N Cu-Ti-S and 4N Cu-Cr-Ni-Ag-S samples,

with the size of the CrS phase notably smaller than that of the TiS phase. Meanwhile, no Ni and Ag precipitates were found in the 4N Cu-Cr-Ni-Ag-S samples.

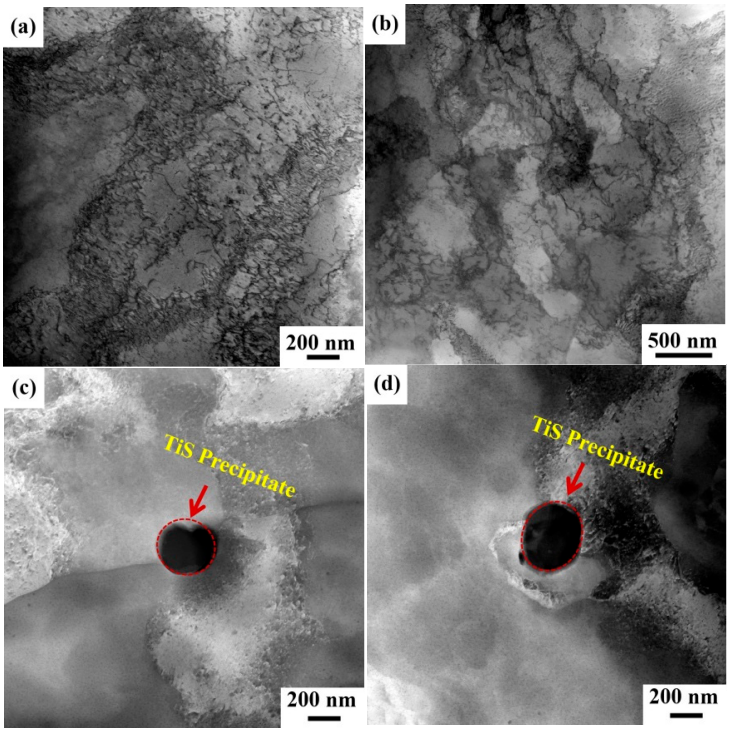

Figure 10. Dislocation and precipitated phase analysis of cold-rolled-state 4N Cu-Ti-S: (**a**) dislocation wall; (**b**) dislocation cells; (**c**) HAADF-STEM images at the grain boundary; and (**d**) HAADF-STEM images within the grains.

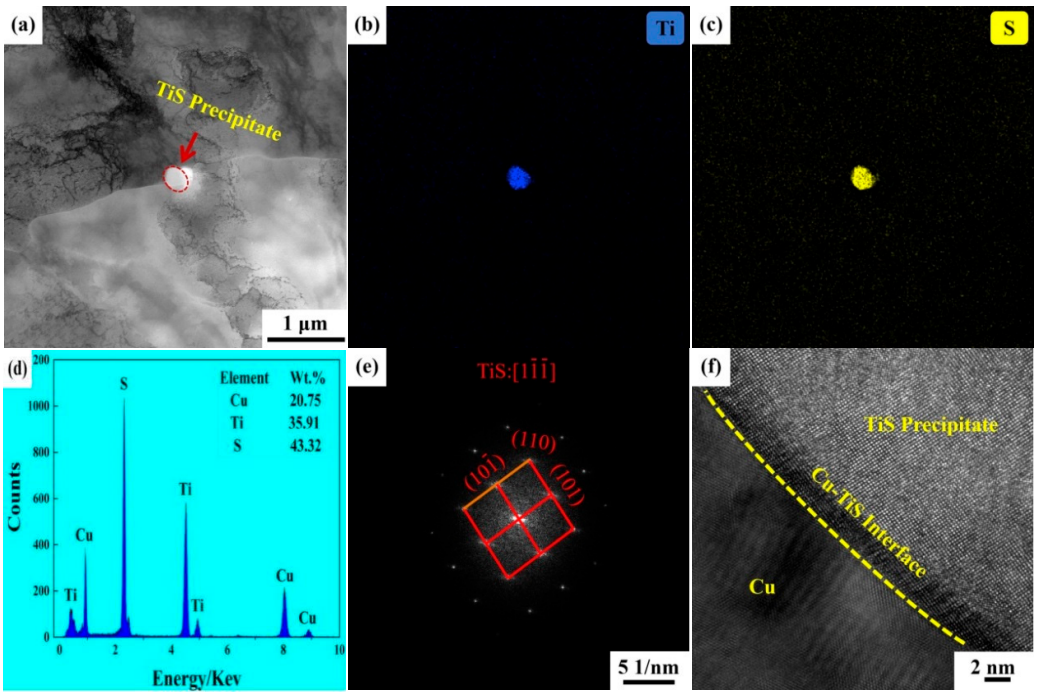

Figure 11. Precipitated phase analysis of cold-rolled 4N Cu-Ti-S at the grain boundary: (**a**) BF-TEM image; (**b**) EDS surface scan of titanium; (**c**) EDS surface scan of sulfur elements; (**d**) EDS spot scanning of precipitated phase; (**e**) SAD image of precipitated phase; and (**f**) TEM high-resolution morphology of the interface between the TiS phase and Cu matrix.

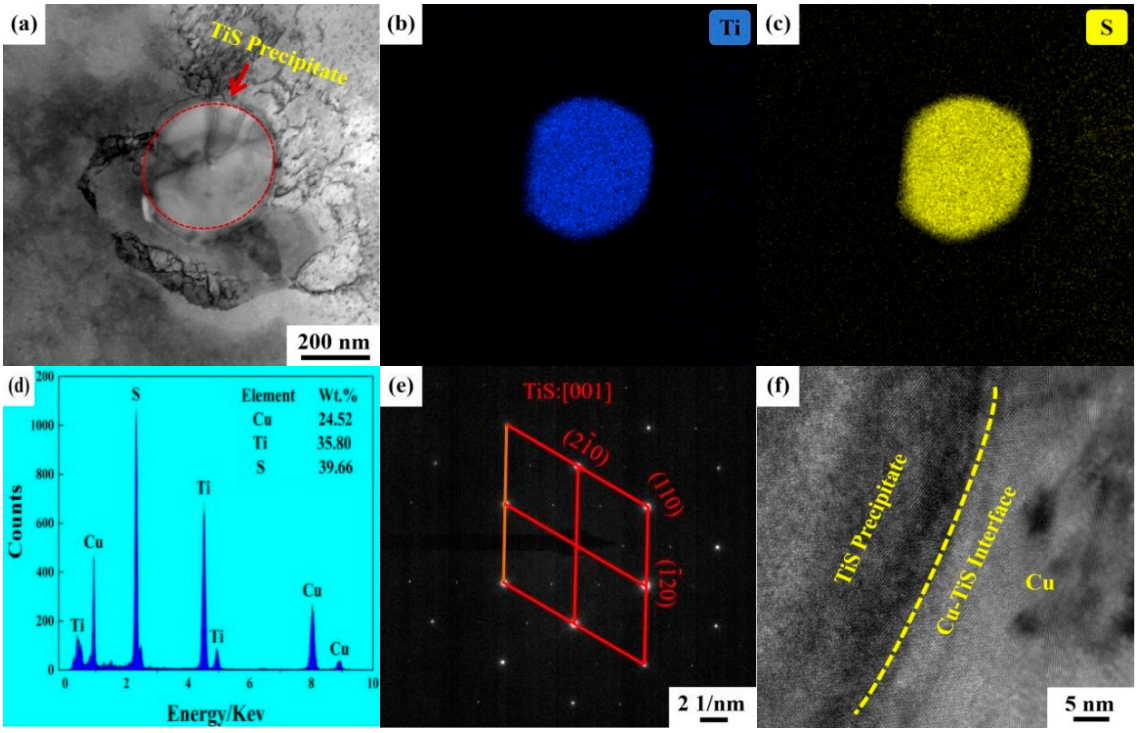

Figure 12. Precipitated phase analysis of cold-rolled 4N Cu-Ti-S within the grain boundary: (**a**) BF-TEM image; (**b**) EDS surface scan of titanium; (**c**) EDS surface scan of sulfur elements; (**d**) EDS spot scanning of precipitated phase; (**e**) SAD image of precipitated phase; and (**f**) TEM high-resolution morphology of the interface between the TiS phase and Cu matrix.

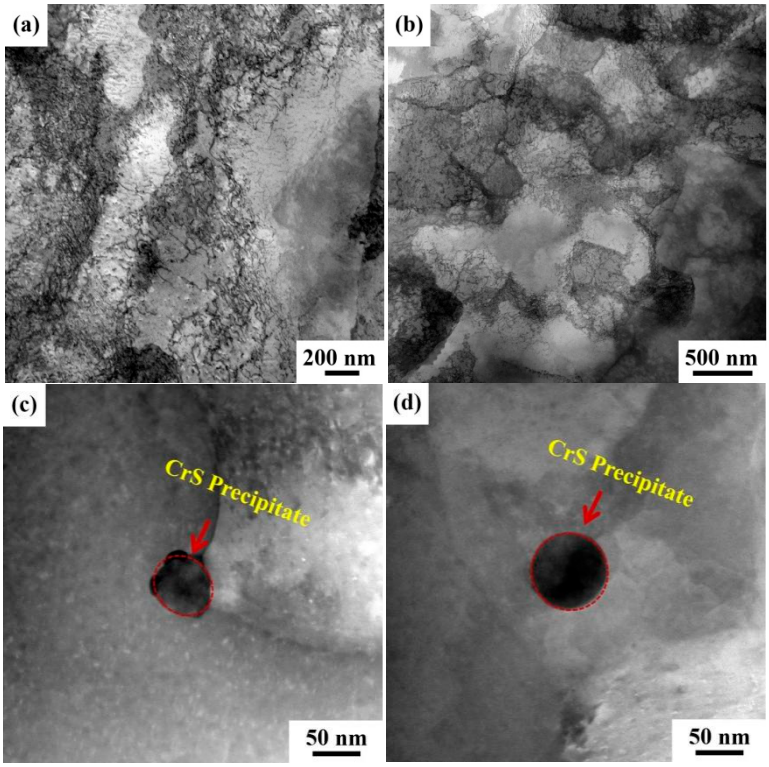

Figure 13. Dislocation and precipitated phase analysis of cold-rolled-state 4N Cu-Cr-Ni-Ag-S: (**a**) dislocation wall; (**b**) dislocation cells; (**c**) HAADF-STEM images at the grain boundary; and (**d**) HAADF-STEM images within the grain boundary.

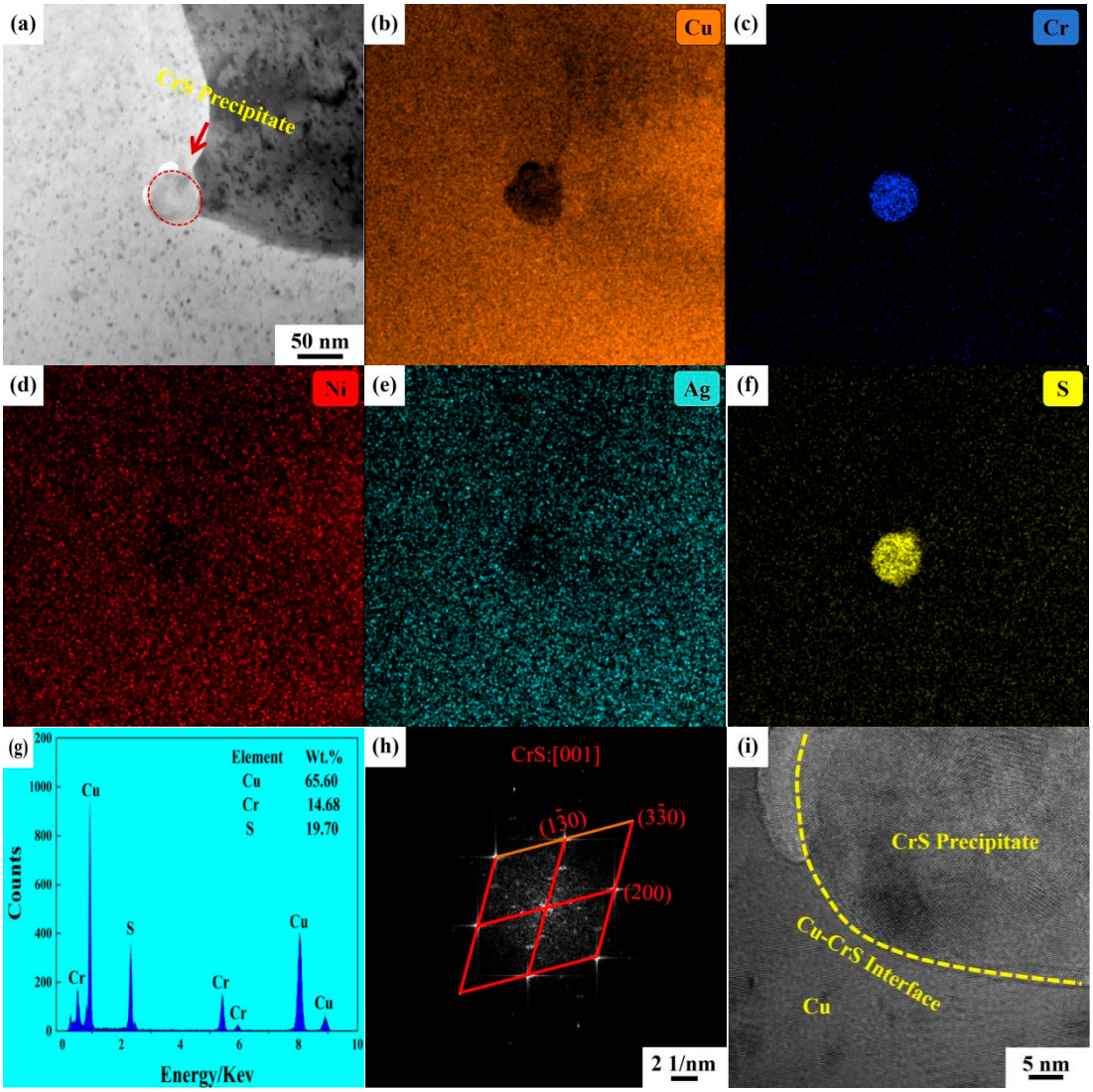

Figure 14. Precipitated phase analysis of cold-rolled 4N Cu-Cr-Ni-Ag-S at the grain boundary: (**a**) BF-TEM image; (**b**) EDS surface scan of copper elements; (**c**) EDS surface scan of chromium elements; (**d**) EDS surface scan of nickel elements; (**e**) EDS surface scan of silver elements; (**f**) EDS surface scan of sulfur elements; (**g**) EDS spot scanning of precipitated phase; (**h**) SAD image of precipitated phase; and (**i**) TEM high-resolution morphology of the interface between the CrS phase and Cu matrix.

Figure 10 shows the distribution of dislocations and precipitated phases in cold-rolled 4N Cu-Ti-S. As depicted in Figure 10a,b, bright-field scanning transmission electron microscopy reveals an increase in dislocation density due to cold-rolling with large deformation. The dislocations accumulate and intertwine, forming dislocation walls and cells within the grain. In Figure 10c,d, high-angle annular dark-field scanning transmission electron microscopy reveals the distribution of precipitates formed in 4N Cu-Ti-S on and within the grain boundaries, with some precipitates also anchored to the dislocation walls. These precipitates exhibit clear ellipsoidal or spherical shapes, with a size of approximately 267 nm at the grain boundary and about 354 nm within the grains.

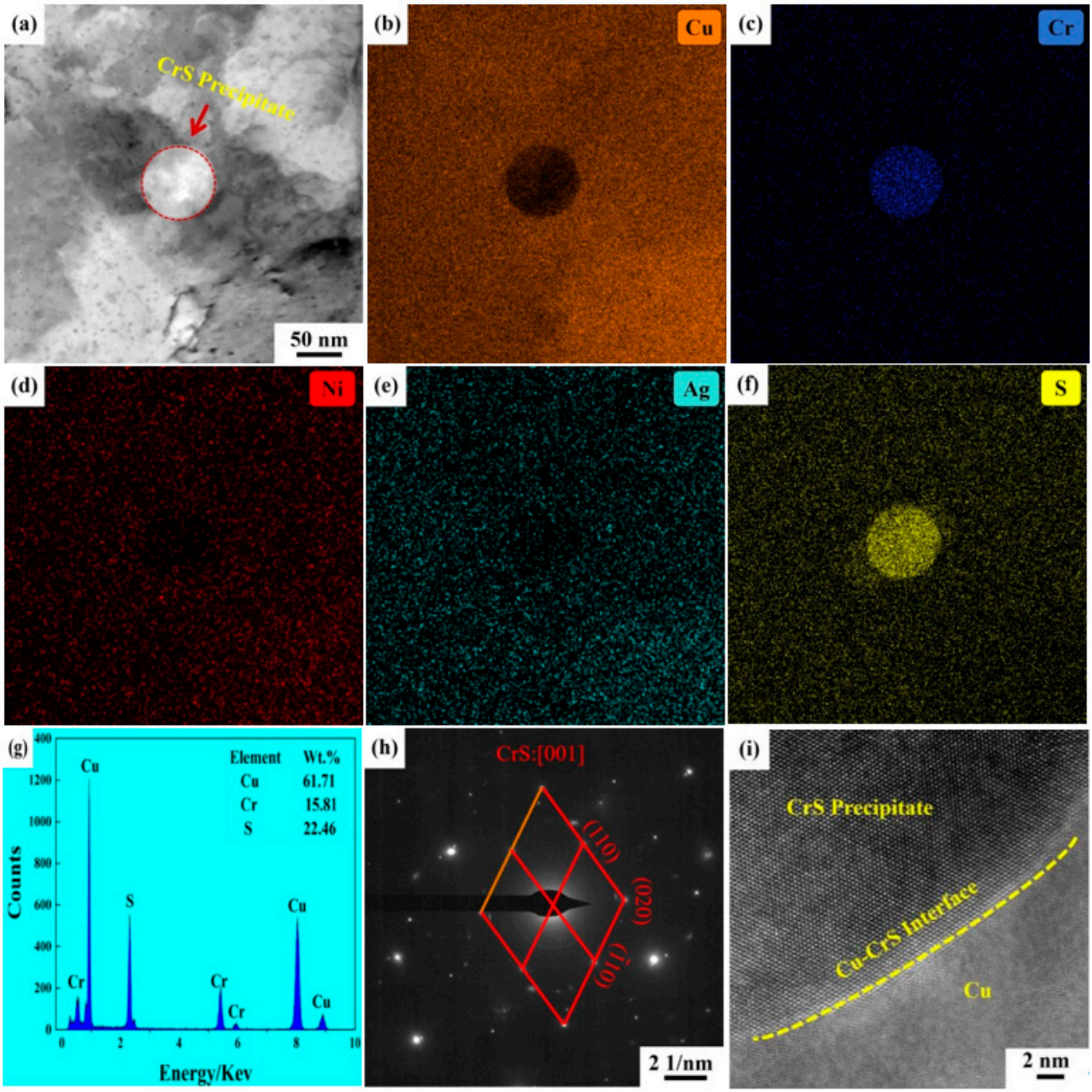

Figure 15. Precipitated phase analysis of cold-rolled 4N Cu-Cr-Ni-Ag-S within the grain boundary: (**a**) BF-TEM image; (**b**) EDS surface scan of copper elements; (**c**) EDS surface scan of chromium elements; (**d**) EDS surface scan of nickel elements; (**e**) EDS surface scan of silver elements; (**f**) EDS surface scan of sulfur elements; (**g**) EDS spot scanning of precipitated phase; (**h**) SAD image of precipitated phase; and (**i**) TEM high-resolution morphology of the interface between the CrS phase and Cu matrix.

Figures 11 and 12 show the typical TEM characteristics of the TiS phase in 4N Cu-Ti-S on the grain boundary and within the grains, respectively. As seen in Figures 11 and 12a–d, the precipitated phases of 4N Cu-Ti-S at the grain boundary and within the grains are TiS phases. The electron diffraction analysis of Figures 11 and 12e confirms that these precipitated phases exhibit a hexagonal structure. Additionally, Figures 11 and 12f display

high-resolution TEM morphologies at the interface between the TiS phase and Cu matrix. The lattice mismatch between the precipitated phase and Cu matrix interface is calculated using Formula (1):

$$\delta_{(hkl)_{M_xS}}^{(hkl)_{Cu}} = \frac{\left|d[hkl]_{Cu} - d[hkl]_{M_xS}\right|}{d[hkl]_{M_xS}} \times 100\% \quad (1)$$

where δ: mismatch between compound and the Cu matrix;

$(hkl)_{Cu}$: low exponential crystal face of the Cu matrix;

$(hkl)_{M_xS}$: low exponential crystal face of the M_xS phase;

d[hkl]: (hkl) crystal face spacing.

The lattice mismatch between the precipitated TiS phase and Cu matrix at the grain boundary is as follows:

$$\delta = \frac{|0.2366 - 0.1802|}{0.1802} \times 100\% = 31.30\% \quad (2)$$

The lattice mismatch between the precipitated TiS phase and Cu matrix within the grain boundary is as follows:

$$\delta = \frac{|0.2344 - 0.1768|}{0.1768} \times 100\% = 32.58\% \quad (3)$$

The results show that the interface between the precipitated phase and the copper matrix is non-coherent. In a cold-rolled state, the precipitates in 4N Cu-Ti-S are distributed at the grain boundary and within the grain boundary. Particularly, the precipitates distributed at the grain boundary can effectively impede grain boundary migration, contributing to the good thermal stability of 4N Cu-Ti-S at high temperatures.

Figure 13 shows the dislocation and precipitated phase distribution of 4N Cu-Cr-Ni-Ag-S in a cold-rolled state. As shown in Figure 13a,b, bright-field scanning transmission electron microscopy reveals that cold-rolling induces an increase in dislocation density, resulting from large deformation. The dislocations pile up to form a dislocation wall, with these walls intertwining to create dislocation cells. As shown in Figure 13c,d, under high-angle annular dark-field scanning transmission electron microscopy, the precipitates formed in 4N Cu-Cr-Ni-Ag-S are distributed at the grain boundary and within the grains, exhibiting a clearly spheroidal morphology. The size of the precipitated phase is small, approximately 55 nm at the grain boundary and about 80 nm within the grain boundary.

Figures 14 and 15 show the typical TEM characteristics of the CrS phase in 4N Cu-Cr-Ni-Ag-S at the grain boundary and within the grain boundary, respectively. Based on the EDS surface map and EDS point map of elements in Figures 14 and 15a–g, it is observed that the precipitated phase of 4N Cu-Cr-Ni-Ag-S consists of Cr and S elements at both the grain boundary and within the boundary, while Ni and Ag elements are uniformly distributed in the Cu matrix without being found on the precipitated phase. Electron diffraction analysis confirms that these precipitated phases are monoclinal CrS phases. Figures 14 and 15i depict the high-resolution TEM morphologies at the interface between the TiS phase and Cu matrix. The lattice mismatch between the precipitated phase and Cu matrix interface is calculated according to Formula (1).

The lattice mismatch between the precipitated CrS phase and Cu matrix at the grain boundary is as follows:

$$\delta = \frac{|0.2383 - 0.1739|}{0.1739} \times 100\% = 37.03\% \quad (4)$$

The lattice mismatch between the precipitated CrS phase and Cu matrix within the grain boundary is as follows:

$$\delta = \frac{|0.1812 - 0.2918|}{0.2918} \times 100\% = 37.90\% \quad (5)$$

The results indicate that the precipitated phase exhibits a non-coherent relationship with the copper matrix interface. The precipitates generated in cold-rolled 4N Cu-Cr-Ni-Ag-S also have very small sizes. The size of 4N Cu-Cr-Ni-Ag-S precipitates is 0.2 times smaller than that of 4N Cu-Ti-S precipitates, suggesting that the former exerts a stronger pinning force on grain boundary migration. Furthermore, its thermal stability surpasses that of 4N Cu-Ti-S at high temperatures.

In summary, the enhancement of thermal stability in Cu-Ti-S and Cu-Cr-Ni-Ag-S microalloyed pure copper is primarily attributed to the formation of a hexagonal-structured TiS phase, monoclinic-structured CrS phase, and the solid solution of Ni and Ag solutes. The mechanism illustrating how trace alloying elements influence the thermal stability of pure copper is illustrated in Figure 16. Trace alloying elements Ti and Cr can react with an impurity element, S, in the pure copper matrix to form the TiS phase and CrS phase, respectively. These phases exhibit a non-coherent relationship with the matrix and exert a pinning effect at high temperatures, thereby improving the thermal stability of grain size in pure copper and transforming the impurity element, S, into beneficial forms. Additionally, Cu-Cr-Ni-Ag-S exhibits superior thermal stability compared to Cu-Ti-S due to the smaller size of the CrS phase in a monoclinic structure as opposed to the TiS phase in a hexagonal structure. Previous studies [43] have indicated that the pinning force of precipitation relative to grain boundary migration is inversely proportional to its size. Thus, introducing more precipitated phases into the copper matrix results in higher thermal stability when these phases are smaller. Furthermore, trace amounts of Ni and Ag dissolved in copper create a solute dragging effect that cooperatively enhances the thermal stability of Cu-Cr-Ni-Ag pure copper; however, due to their scattering effect on electron transport within copper, Ni and Ag atoms reduce its conductivity to some extent.

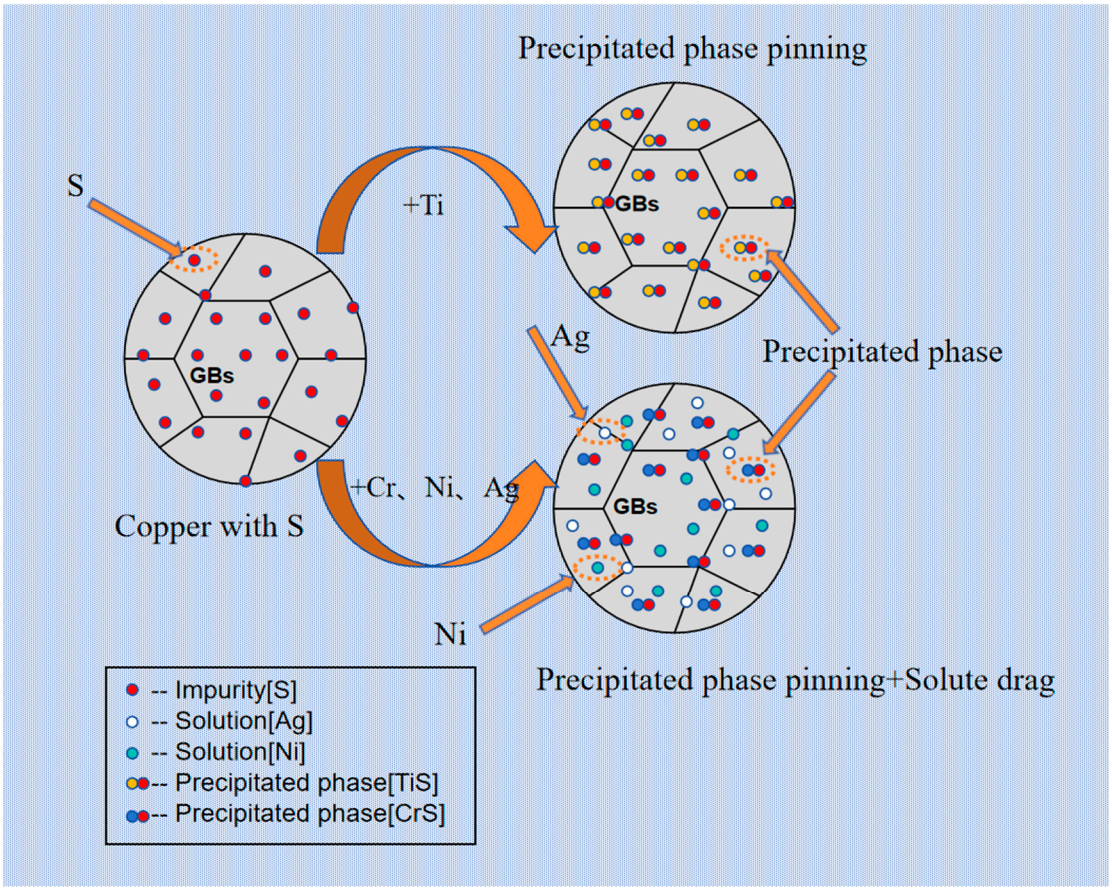

Figure 16. Schematic diagram of the mechanism of action of trace alloying elements on the thermal stability of pure copper.

4. Conclusions

In this chapter, the impact of trace elements on the thermal stability of cold-rolled pure copper was investigated through an analysis of grain size following high-temperature treatment at 900 °C/30 min. Furthermore, the mechanism for improving the thermal stability of pure copper grain size was established. The primary conclusions are as follows:

1. After the addition of trace elements, the conductivity of pure copper remains high, especially the conductivity of the Cu-Ti-S sample, essentially equivalent to that of the Cu sample. The conductivities of 4N Cu, 4N Cu-Ti-S, and 4N Cu-Cr-Ni-Ag-S are 100.7% IACS, 100.2% IACS, and 98.5% IACS, respectively. This can be primarily attributed to the fact that trace transition elements Ti and Cr can react with S in copper to form the TiS phase and CrS phase, effectively reducing the solid solution of trace elements in the copper matrix and minimizing electron wave scattering, thus having little impact on electrical conductivity. However, a significant decrease in electrical conductivity was observed for 4N Cu-Cr-Ni-Ag-S due to the solid solution of trace Ni and Ag elements.
2. The thermal stability of grain size in cold-rolled pure copper can be significantly improved by adding trace elements, with the order of thermal stability being Cu-Cr-Ni-Ag-S > Cu-Ti-S > Cu. Following heat treatment at 900 °C/30 min, the average grain sizes of 4N Cu, 4N Cu-Ti-S, and 4N Cu-Cr-Ni-Ag-S were 200.24 μm, 83.83 μm, and 31.08 μm, respectively. In particular, the cold-rolled 4N Cu-Cr-Ni-Ag exhibited the best thermal stability with a grain size of 31.08 μm after high-temperature treatment.
3. The enhancement of thermal stability following the addition of trace elements is primarily attributed to the pinning effect of TiS and CrS phases, as well as the solute drag exerted by Ni and Ag. The trace elements Ti and Cr can react with an impurity element, S, to form the hexagonal-structure TiS phase and monoclinic-structure CrS phase, which are distributed at the grain boundary and within the grain boundary. They exhibit a non-coherent relationship with the copper matrix interface, producing strong pinning force at high temperature and hindering grain boundary migration. In particular, CrS is smaller and more numerous than TiS, which contributes to enhancing the thermal stability of pure copper. Additionally, trace Ni and Ag solid solutions in copper can produce a solute drag effect that further improves its thermal stability.

Author Contributions: Conceptualization, H.L.; Methodology, H.L. and Y.L.; Validation, J.D., S.L. and W.L.; Formal analysis, W.L. and Y.L.; Investigation, S.L.; Writing—original draft, J.D. and S.L.; Writing—review & editing, J.D.; Supervision, H.L.; Funding acquisition, H.L. All authors have read and agreed to the published version of the manuscript.

Funding: This research was funded by Provincial State-owned Capital Operation Budget Expenditure Project in 2024-Development of key technologies for clean control of advanced conductor materials (No. Yucaiqi [2024]10); Joint Fund of Henan Province Science and Technology R&D Program-Control technology and industrialization of impurity elements in high performance copper based materials (No. 235200810004); Luoyang major science and technology innovation special project (No. 2201017A); Henan key research and development project (No. 221111230600); National Natural Science Foundation of China (No. 52071133); High-level Talent Research Start-up Project Funding of Henan Academy of Sciences (No. 242017002).

Institutional Review Board Statement: Not applicable.

Informed Consent Statement: Not applicable.

Data Availability Statement: The data are available in a publicly accessible repository.

Conflicts of Interest: The authors declare no conflicts of interest.

References

1. Gao, Y.M.; Liu, Y.; Feng, K.J.; Ma, J.Q.; Miao, Y.J.; Xu, B.R.; Pan, K.M.; Akiyoshi, O.; Wang, G.X.; Zhang, K.K.; et al. Emerging WS_2/WSe_2@graphene nanocomposites: Synthesis and electrochemical energy storage applications. *Rare Met.* **2024**, *43*, 1–19. [CrossRef]
2. Liu, Y.; Feng, K.; Han, J.; Wang, F.; Xing, Y.; Tao, F.; Li, H.; Xu, B.; Ji, J.; Li, H. Regulation of Zn^{2+} solvation shell by a novel N-methylacetamide based eutectic electrolyte toward high-performance zinc-ion batteries. *J. Mater. Sci. Technol.* **2025**, *211*, 53–61. [CrossRef]
3. Li, T.; Wang, Y.; Yang, M.; Hou, H.; Wu, S. High strength and conductivity copper/graphene composites prepared by severe plastic deformation of graphene coated copper powder. *Mater. Sci. Eng. A* **2021**, *826*, 141983. [CrossRef]
4. Zhou, X.; Hu, Z.; Yi, D. Enhancing the oxidation resistance and electrical conductivity of alumina reinforced copper-based composites via introducing Ag and annealing treatment. *J. Alloys Compd.* **2019**, *787*, 786–793. [CrossRef]
5. Li, Z.; Xiao, Z.; Jiang, Y.B.; Lei, Q.; Xie, J.X. Composition design, phase transition and fabrication of copper alloys with high strength and electrical conductivity. *Chin. J. Nonferrous Met.* **2019**, *29*, 2009–2049.
6. Lin, H.R.; Shao, H.F.; Zhang, Z.J.; Yang, H.J.; Sun, J.C.; Zhang, L.B.; Zhang, Z.F. Stress relaxation behaviors and mechanical properties of precipitation strengthening copper alloys. *J. Alloys Compd.* **2021**, *861*, 158537. [CrossRef]
7. Akhtar, S.S.; Kareem, L.T.; Arif, A.F.M.; Siddiqui, M.U.; Hakeem, A.S. Development of a ceramic-based composite for direct bonded copper substrate. *Ceram. Int.* **2017**, *43*, 5236–5246. [CrossRef]
8. Gao, W.; Belyakov, A.; Miura, H.; Sakai, T. Dynamic recrystallization of copper polycrystals with different purities. *Mater. Sci. Eng. A* **1999**, *265*, 233–239. [CrossRef]
9. Orlova, D.K.; Chashchukhina, T.I.; Voronova, L.M.; Degtyarev, M.V.; Krasnoperova, Y.G. Effect of impurities on dynamic recrystallization in copper deformed in bridgman anvils. *Diagn. Resour. Mech. Mater. Struct.* **2015**, 90–98. [CrossRef]
10. Jakani, S.; Baudin, T.; de Novion, C.H.; Mathon, M.H. Effect of impurities on the recrystallization texture in commercially pure copper-ETP wires. *Mater. Sci. Eng. A* **2007**, *456*, 261–269. [CrossRef]
11. Chen, B.; Wang, D.; Jin, H. Study of pure copper ceramic CCL fabrication using two-step magnetron sputtering. *VACCUM* **2016**, *53*, 22–24.
12. Lu, Q.; Liu, Y.K.; Qiao, Z.Z.; Liu, L.J.; Gao, L. Research status and new progress of ceramic substrate. *Semicond. Technol.* **2021**, *46*, 257–268.
13. Qin, D.C.; Li, B.Z.; Xiao, Y.L. Research situation and development trend of ceramic metallization. *Mater. Rep.* **2017**, *31*, 277–281.
14. Fan, B.; Zhao, L.; Xie, Z. Progress in research and application of joining of ceramics and metals. *J. Ceram.* **2020**, *41*, 9–21.
15. Liu, A.; Lu, C.; Duan, G. Application of High Performance Copper Alloy Strip in Automotive Connectors. *Copp. Eng.* **2018**, *2*, 13–16.
16. Zhu, M.; Guo, X. Study on softening resistance of pure copper. *China Met. Bull.* **2020**, *6*, 88–89.
17. Li, M.; Zhang, Y.; Wang, W. Effects of trace hafnium on microstructure and properties of copper and copper-chromium alloys. *Heat Treat. Met.* **2018**, *43*, 23–30.
18. Atwater, M.A.; Roy, D.; Darling, K.A.; Butler, B.G.; Scattergood, R.O.; Koch, C.C. The thermal stability of nanocrystalline copper cryogenically milled with tungsten. *Mater. Sci. Eng. A* **2012**, *558*, 226–233. [CrossRef]
19. Lu, T.; Chen, C.; Li, P.; Zhang, C.; Han, W.; Zhou, Y.; Suryanarayana, C.; Guo, Z. Enhanced mechanical and electrical properties of in situ synthesized nano-tungsten dispersion-strengthened copper alloy. *Mater. Sci. Eng. A* **2021**, *799*, 140161. [CrossRef]
20. Rajkovic, V.; Bozic, D.; Jovanovic, M.T. Effects of copper and Al_2O_3 particles on characteristics of Cu–Al_2O_3 composites. *Mater. Des.* **2010**, *31*, 1962–1970. [CrossRef]
21. Yuan, Y.; Tang, W. Microstructure and properties of Cu-Al_2O_3 dispersion strengthened copper alloy contact wire. *Trans. Mater. Heat Treat.* **2020**, *41*, 33–38.
22. Cheng, J.; Wang, M. Research status of dispersion strengthened copper alloys with high strength, high conductivity and high heat resistance. *Mater. Rep.* **2004**, *2*, 38–41.
23. Chen, Y.; Wei, M.; Duan, P.; Liu, P. Effect of different microalloying elements on microstructure and properties of Cu-Cr-Zr alloy. *Spec. Cast. Nonferrous Alloys* **2007**, *5*, 404–406+328.
24. Fang, H.; Liu, P.; Chen, X.; Zhou, H.; Fu, S.; Liu, K.; Liu, H.; Guo, W. Effect of Ti addition on the microstructure and properties of Cu–Cr alloy. *Mater. Sci. Technol.* **2021**, *37*, 672–681. [CrossRef]
25. Peng, H.; Xie, W.; Chen, H.; Wang, H.; Yang, B. Effect of micro-alloying element Ti on mechanical properties of Cu–Cr alloy. *J. Alloys Compd.* **2021**, *852*, 157004. [CrossRef]
26. Anderson, K.R.; Groza, J.R.; Dreshfield, R.L.; Ellis, D. Microstructural evolution and thermal stability of precipitation-strengthened Cu-8Cr-4Nb alloy. *Mater. Sci. Eng. A* **1993**, *169*, 167–175. [CrossRef]
27. Peng, L.M.; Mao, X.M.; Xu, K.D.; Ding, W.J. Property and thermal stability of in situ composite Cu–Cr alloy contact cable. *J. Mater. Process. Tech.* **2004**, *166*, 193–198. [CrossRef]
28. Zhang, Z.Y.; Sun, L.X.; Tao, N.R. Raising thermal stability of nanograins in a CuCrZr alloy by precipitates on grain boundaries. *J. Alloys Compd.* **2021**, *867*, 159016. [CrossRef]
29. Eguchi, H.; Arai, M.; Fujii, S.; Fujita, M.; Takayama, Y. Effect of Ag Content on Grain Growth during Reversion in Precipitation Hardened Cu-Cr-Zr-Ag Alloys. In Proceedings of the 8th Pacific Rim International Congress on Advanced Materials and Processing, Waikoloa, HI, USA, 4–9 August 2013; Springer International Publishing: Cham, Switzerland, 2016; pp. 2277–2284.

30. Li, X.; Deng, J.; Fu, H.; Chen, J. A study of process on improving heat resistance of copper strip. *Nonferrous Met. Process.* **2014**, *43*, 25–29.
31. Toguchi, S.; Yamamoto, Y.; Kodama, K.; Kato, K.; Konochi, T. Oxygen-Free Copper Plate and Ceramic Wiring Substrate. Patent CN201810564074.6, 30 October 2020.
32. Suzuki, H.; Kanno, M.; Maeda, T. Effects of a Small Addition of Transition Elements on the Heat-Resisting and Electrical Properties of Cold-Worked Pure Copper. *J. Jpn. Inst. Met.* **1984**, *48*, 209–213. [CrossRef]
33. Hori, S.; Tai, H.; Katayama, H. Recrystallization Temperatures of Dilute Copper Alloys. *Nippon. Kinzoku Gakkaishi* **1981**, *45*, 1223–1228.
34. Suzuki, H.; Kanno, M. Increase of recrystallization rate of pure copper by the trace addition of Ti, Zr or V. *Tetsu-Hagané* **1984**, *70*, 1977–1983. [CrossRef] [PubMed]
35. Suzuki, H.; Kanno, M. Effect of a small addition of transition elements on annealing characteristics of cold-worked pure copper. *Trans. Jpn. Inst. Met.* **1985**, *26*, 69–77. [CrossRef]
36. Chiu, W.L.; Hung, Y.T.; Lee, O.H.; Ou-Yang, T.Y.; Chang, H.H.; Lo, W.C. Improvement of nanotwinned copper thermal stability for high temperature heterogeneous integration. In Proceedings of the 2021 International Symposium on VLSI Technology, Systems and Applications (VLSI-TSA), Hsinchu, Taiwan, 19–22 April 2021; IEEE: New York, NY, USA, 2021; pp. 1–2.
37. Woo, P. Thermal Stability of Nanocrystalline Copper for Potential Use in Printed Wiring Board Applicatoins. Ph.D. Thesis, University of Toronto, Toronto, ON, Canada, 2011.
38. Li, W.; Shen, Y.; Xie, C. High thermal stability of submicron grained Cu processed by asymmetrical rolling. *Mater. Des.* **2016**, *105*, 404–410. [CrossRef]
39. Kuroda, Y.; Jiu, J.; Sasakawa, Y.; Aoyama, Z. Manufacturing Method of Low Concentration Copper Alloy Material and Low Concentration Copper Alloy Material with Excellent Hydrogen Embrittlement Resistance. Patent CN201110326773.5, 30 March 2016.
40. Ren, J.; Meng, Q.; Wang, Y.; Zhao, J.; Zang, J.; Zeng, L.; Pan, F. The Production Method and Equipment of Grain Coarsening Resistant Copper Ingot and Grain Coarsening Resistant Copper . Patent CN202111609219.8, 1 August 2022.
41. Bikowski, A.; Ellmer, K. Analytical model of electron transport in polycrystalline, degenerately doped ZnO films. *J. Appl. Phys.* **2014**, *116*, 143704. [CrossRef]
42. Ishibe, T.; Tomeda, A.; Watanabe, K.; Kamakura, Y.; Mori, N.; Naruse, N.; Mera, Y.; Yamashita, Y.; Nakamura, Y. Methodology of thermoelectric power factor enhancement by controlling nanowire interface. *ACS Appl. Mater. Interfaces* **2018**, *10*, 37709–37716. [CrossRef]
43. Aoyama, S.; Kanno, M. Effects of small additions of lead, sulphur and oxygen on annealing characteristics of cold-drawn pure copper. *J. Mater. Sci.* **1996**, *31*, 2393–2399. [CrossRef]